HHS Public Access

Author manuscript

Neuron. Author manuscript; available in PMC 2024 May 03.

Published in final edited form as:

Neuron. 2023 May 03; 111(9): 1381–1390.e6. doi:10.1016/j.neuron.2023.02.029.

Downregulation of Hsp90 and the Antimicrobial Peptide Mtk Suppresses Poly(GR)-Induced Neurotoxicity in *C9ORF72*-ALS/FTD

Soojin Lee[1], **Yong-Woo Jun**[1], **Gabriel R. Linares**[2], **Brandon Butler**[2], **Yeliz Yuva-Adyemir**[1,†], **Jill Moore**[3], **Gopinath Krishnan**[1], **Bryan Ruiz-Juarez**[2], **Manuel Santana**[2], **Marine Pons**[1], **Neal Silverman**[4], **Zhiping Weng**[3], **Justin Ichida**[2], **Fen-Biao Gao**[1,*,#]

[1]Department of Neurology, UMass Chan Medical School, Worcester, MA 01605, USA

[2]Department of Stem Cell Biology and Regenerative Medicine, Eli and Edythe Broad Center for Regenerative Medicine and Stem Cell Research, University of Southern California, Los Angeles, CA, USA

[3]Program in Bioinformatics and Integrative Biology, UMass Chan Medical School, Worcester, 01605 USA

[4]Division of Infectious Diseases and Immunology, Department of Medicine, University of Massachusetts Chan Medical School, Worcester, MA 01605, USA

SUMMARY

GGGGCC repeat expansion in *C9ORF72* is the most common genetic cause of amyotrophic lateral sclerosis (ALS) and frontotemporal dementia (FTD). Repeat RNAs can be translated into dipeptide repeat proteins, including poly(GR), whose mechanisms of action remain largely unknown. In an RNA-seq analysis of poly(GR) toxicity in *Drosophila*, the antimicrobial peptide (AMP) gene *metchnikowin* (*Mtk*) was greatly activated and whose knockdown in the eye or in all neurons suppressed poly(GR) neurotoxicity, suggesting a cell-autonomous role of Mtk in neurodegeneration. We also found that Hsp90 knockdown decreased poly(GR)-induced activation

*To whom correspondence should be addressed. fen-biao.gao@umassmed.edu. #Lead Contact. fen-biao.gao@umassmed.edu.
†Present address: CAMP4 Therapeutics, Cambridge, MA 02139

AUTHOR CONTRIBUTIONS

Project initiation: F.-B.G. and S.L.; conceptualization, F.-B.G., S.L. and N.S.; investigations, S.L., Y.-W.J., G.K., Y.Y.-A., G.L., B.R.J., M.S. and M.P.; formal analysis, S.L., J.M. and Z.W.; funding acquisition, F.-B.G., J.I. and Z.W.; supervision, F.-B.G.; writing - original draft, F.-B.G., S.L., G.L. and J.M.; writing - review & editing, F.-B.G. and S.L.

INCLUSION AND DIVERSITY STATEMENT

One or more of the authors of this paper self-identifies as an underrepresented ethnic minority in their field of research or within their geographical location. One or more of the authors of this paper self-identifies as a gender minority in their field of research. One or more of the authors of this paper received support from a program designed to increase minority representation in their field of research.

SUPPLEMENTAL INFORMATION

Supplemental information includes four figures that can be found with this article online. Table S1 titled “The genotypes of fly lines used in this study (Related to the STAR Methods)” and Table S2 titled “Primers used in this study (Related to STAR Methods)” can also be found online.

of Mtk and partially rescued both poly(GR) toxicity in flies and neurodegeneration in *C9ORF72* neurons derived from induced pluripotent stem cells (iPSCs). Upregulation of Hsp90 and Mtk is mediated by topoisomerase II (TopoII) whose downregulation also suppresses poly(GR) toxicity in fly neurons and neurodegeneration of patient neurons. These results identify Hsp90 and some AMPs as potential therapeutic targets for *C9ORF72*-ALS/FTD.

eTOC

Using fruitflies and neurons derived from stem cells of patients with ALS/FTD as their experimental systems, Lee et al. found that knockdown of three proteins that are likely function in a related pathway partially suppresses the neurotoxicity of poly(GR), a pathological protein in ALS/FTD.

INTRODUCTION

Amyotrophic lateral sclerosis (ALS) and frontotemporal dementia (FTD) are major devastating neurodegenerative diseases. ALS and FTD are considered to be part of a spectrum disorder because of their shared genetic causes, the most common being a *GGGGCC* (G_4C_2) repeat expansion in the first intron of *C9ORF72*[1,2]. Repeat RNAs and adjacent intronic sequences transcribed from both sense and antisense directions can be translated into abnormal proteins containing different dipeptide repeats such as poly(GR) and poly(GA)[3–5]. In *C9ORF72* patient brains, the pattern of poly(GR) expression appears to correlate with neurodegeneration[6–8], suggesting a central role for poly(GR) in the molecular pathogenesis of *C9ORF72*-ALS/FTD.

G_4C_2 repeats and DPR proteins cause cellular toxicity in numerous cellular and animal models through impacting multiple molecular pathways[9–11]. For instance, nucleocytoplasmic transport is disrupted by both toxic G_4C_2 repeat-containing RNA and arginine-containing DPR proteins[12–15]. Poly(GR) and poly(PR) bind to motor complexes and microtubules resulting in compromised axonal transport[16]. These DPR proteins also inhibit global protein synthesis by binding to ribosomes[17–20]. Another important pathway disrupted by arginine-containing DPR proteins is DNA damage. Control human neurons ectopically expressing poly(GR) or aged *C9ORF72* patient neurons differentiated from induced pluripotent stem cell (iPSC) lines show increases in DNA damage and in the levels of both total and phosphorylated p53[18,21]. Importantly, knocking down p53 dramatically suppresses poly(GR) or poly(PR) toxicity in *Drosophila*[18] or cultured mammalian neurons[21]. Moreover, downregulation of *Ku80*, a key DNA damage repair gene upstream of p53 activation, also rescues poly(GR) toxicity in *Drosophila* and neurodegeneration in *C9ORF72* iPSC-derived motor neurons[22]. Despite this progress, it remains to be determined what other suppressor genes and parallel molecular pathways contribute to poly(GR) toxicity.

In this study, we set out to perform an RNA-seq analysis of poly(GR) toxicity in *Drosophila* and identified the antimicrobial peptide gene *metchnikowin (Mtk)* as a novel contributing factor to poly(GR) toxicity in *Drosophila*. We further showed that knockdown of Hsp90 decreased Mtk level and genetic or antisense oligonucleotide (ASO) knockdown of Hsp90

and its transcriptional regulator TopoII rescued neurodegeneration in both fly and iPSC-derived human neuron models of *C9ORF72*-ALS/FTD.

RESULTS

Overactivation of the Antimicrobial Peptide Gene *Metchnikowin* Contributes to Poly(GR)-Induced Neurotoxicity in *Drosophila*

Drosophila models have been widely used to understand pathogenic mechanisms of various neurodegenerative diseases[23]. To further understand the molecular mechanisms of poly(GR)-induced neurodegeneration, we performed an RNA-seq analysis in *Drosophila* brains expressing poly(GR) in the neurons. In this experiment, 80 copies of GR (GR_{80}) with a Flag tag at the N-terminus was expressed from a non G_4C_2 sequence using the *UAS-Gal4* system. GR_{80} was expressed in all neurons only at the adult stage after 1-3 days old adult flies were shifted from low temperature 18 °C to high temperature 25 °C[24]. In this fly model, the temperature-sensitive yeast transcription suppressor Gal80 (*$Gal80^{ts}$*) was able to inhibit the pan-neuronal *elav-Gal4* mediated transcription at 18 °C but not at 25 °C. *UAS-Cont-$(GR)_{80}$* expresses *$(GR)_{80}$* mRNA but the start codon AUG is changed into the stop codon UAA, which serves as the negative control[25]. Total RNAs from heads of poly(GR)-expressing flies of four independent crosses were isolated and compared with three groups of control flies (Figure 1A). We identified 52 significantly downregulated genes and 148 upregulated genes in poly(GR)-expressing flies (Figures 1A and 1B). Gene ontology analysis showed dysregulation of genes in several major molecular pathways, including *Ku80* in the nonhomologous end-joining DNA repair pathway (Figure 1C and S1), consistent with our earlier findings in poly(GR)-expressing flies and in *C9ORF72* patient neurons[22,24]. Biological processes enriched in upregulated genes included heat shock–mediated polytene chromosome puffing, defense response to insect, protein refolding, and antibacterial humoral response (Figure 1C and S1). A STRING analysis showed highly interconnected clusters of proteins involved in the stress response and innate immune pathways (Figure 1D).

A number of antimicrobial peptide (*AMP*) genes are significantly upregulated in poly(GR)-expressing flies, such as *Metchnikowin (Mtk)* and *Diptericin B (DptB)* (Figures 1E and S1). To verify the results from RNA-seq, we validated each of the top 6 *AMP* genes using real-time quantitative PCR (RT-qPCR) in flies obtained from a new genetic cross and showed that indeed these *AMP* genes were upregulated in flies expressing poly(GR) (Figure 1F). *AMP* genes are key players in preventing pathogen-induced infections and are upregulated during innate immune responses to infection in animals including humans[26,27], however, the roles of *AMP* genes in animal models of ALS/FTD or other neurodegenerative diseases are poorly understood. To examine whether overactivation of some *AMP* genes contributes to poly(GR) toxicity in flies, we expressed poly(GR) in fly eyes under the control of *GMR-Gal4* at 23 °C and also *$Gal80^{ts}$* to ensure a low level of poly(GR) expression and a modest retinal degeneration phenotype was induced[22]. This phenotype was suppressed by loss of one allele of *Mtk* but not *DptA/B* (Figures 1G and 1I). The loss-of-function of mutant alleles of *Mtk* and *DptB* was confirmed by RT-qPCR analysis (Figure S2A and S2B). *Mtk* reduction by RNAi also suppressed poly(GR) toxicity as evidenced by both the

external eye morphology (Figures 1H and 1I) and internal structures of ommatidium (Figure 1H). Moreover, partial knockdown of *Mtk* using three different RNAi lines in fly neurons also partially rescued the locomotor defect caused by poly(GR) toxicity in a climbing assay and conversely, *Mtk* overexpression in neurons enhanced the locomotor defect (Figure 1J), indicating a cell-autonomous function for *Mtk* in neurodegeneration. The knockdown efficiency of *Mtk* RNAi lines was confirmed by RT-qPCR analysis (Figure S2C). Taken together, overactivation of the *AMP* gene *Mtk* contributes to poly(GR) neurotoxicity in a cell-autonomous manner in this *Drosophila* model of *C9ORF72*-ALS/FTD.

Activation of Mtk Is Mediated by Hsp90 and Partial Knockdown of Hsp90 Suppresses Poly(GR) Toxicity in *Drosophila* and Neurodegeneration in *C9ORF72* IPSC-Derived Motor Neurons

Our RNA-seq analysis revealed that genes encoding many heat shock proteins (Hsps) are also upregulated in poly(GR)-expressing neurons (Figures 1B and 2A). To investigate the involvement of different heat shock proteins in poly(GR) toxicity, we used two independent RNAi lines for each gene and found that partial knockdown of *Hsp23*, *Hsp26* and *Hsp27* enhanced poly(GR) toxicity in the fly eye (Figures S2D and S2E). The RNAi knockdown efficiency for different *Hsp* genes was confirmed by RT-qPCR analysis (Figures S2F–S2J). In contrast, downregulation of Hsp90 activity by a *Hsp90* RNAi greatly suppressed poly(GR) toxicity as quantified by the severity of rough eye phenotype (Figures 2B and 2D). The abnormal internal structure of ommatidium caused by poly(GR) toxicity was also partially rescued by reducing Hsp90 activity (Figure 2B). To confirm this finding, we used two different genetic mutant alleles of *Hsp90* (*Hsp90*^{e6A} and *Hsp90*^{e6D}) and found that partial loss of Hsp90 function indeed rescued poly(GR) toxicity (Figures 2C and 2D). Conversely, *Hsp90* overexpression greatly enhanced poly(GR) toxicity (Figures 2C and 2D). Hsp90 is the most abundant constitutively expressed stress protein in the cells and accounts for 1-2% of total cellular proteins under physiological conditions[28,29] , whose expression is controlled at the transcriptional level by the evolutionarily conserved heat shock transcription factor (Hsf)[30]. Poly(GR) toxicity was also greatly reduced in mutant flies heterozygous for *Hsf* (Figures 2C and 2D). These results are consistent with a previous report demonstrating that upregulation of heat shock genes by Hsf contributes to poly(GR) toxicity in fly models[31]. Hsp90 downregulation does not affect the expression level of poly(GR) protein (Figure 2E), as measured by a Meso Scale Discovery assay[22,32], indicating that the suppressor effect of Hsp90 downregulation on poly(GR) toxicity is not simply due to lower poly(GR) level, rather, it affects a pathway downstream of poly(GR) expression. Due to both Hsp90 and Mtk being suppressors of poly(GR) toxicity, we examined whether Hsp90 acts upstream of Mtk. Indeed, *Hsp90* knockdown attenuated the increased *Mtk* expression in poly(GR)-expressing fly heads (Figure 2F). However, *Hsp90* overexpression by *GMR-Gal4* does not increase *Mtk* level in wildtype flies (Fig. S2K), suggesting regulation of *Mtk* expression by elevated Hsp90 under pathological conditions may be indirect.

To examine whether HSP90 is involved in pathogenesis of *C9ORF72*-ALS/FTD in a human neuron model, we differentiated two *C9ORF72* patient iPSC lines and their isogenic control lines, which had CRISPR/Cas9-mediated deletion of expanded G_4C_2 repeats, into motor

neurons[22]. Consistent with our fly data, HSP90 protein expression level was increased in 3-month-old *C9ORF72* iPSC-derived motor neurons (Figures 2G and 2H). We then investigated neuronal survival using the culture system as previously reported[33]. We tested two different antisense oligonucleotides (ASOs) to reduce *HSP90AA1* expression by about 40% (Figure 2I). After withdrawal of neurotrophic factors, cell death was greater in *C9ORF72*-ALS patient motor neurons than in controls (3 donors per genotype, Figure 2J), as reported[33]. Both *HSP90AA1*-targeted ASOs significantly rescued the neurodegeneration phenotype of *C9ORF72*-ALS/FTD patient motor neurons (Figure 2J), suggesting that *HSP90AA1* is also a novel genetic modifier of *C9ORF72*-related neurotoxicity in human patient neurons.

TopoII Is Also a Genetic Modifier of Poly(GR) Toxicity in *Drosophila* and *C9ORF72* iPSC-Derived Motor Neurons

During our studies of Mtk and Hsp90, we also found that *topoisomerase II* (*TopoII*) knockdown by two different RNAi lines partially rescued poly(GR) toxicity in the adult fly eye, as revealed by external eye morphology (Figures 3A and 3B) or internal structure of ommatidium (Figure 3A). *TopoII* RNAi lines were validated by RT-qPCR analysis (Figure S2L). TopoII is an enzyme that generates a transient double-strand DNA break during replication and transcription[34]. To further confirm this finding, we found that doxorubicin, a TopoII-specific inhibitor used as an anticancer drug[35], did not affect the eye morphology of control flies (data not shown) but partially suppressed the eye degeneration phenotype when fed to poly(GR)-expressing flies in food at a concentration of 1 μM or 10 μM (Figures 3C and 3D). Moreover, neuron-specific knockdown of *TopoII* or *Hsp90* partially rescued locomotor defects of flies with neurons-specific expression of poly(GR) (Figure 3E), indicating a cell-autonomous role for both TopoII and Hsp90 in promoting poly(GR)-induced neurodegeneration. Previously, we reported that downregulation of the DNA damage repair gene *Ku80* or the DNA damage response gene *p53* attenuates poly(GR) toxicity in flies and partially rescues neurodegeneration in *C9ORF72* patient neurons[18,22]. Here we found that downregulation of *TopoII* does not affect poly(GR)-induced increases in the expression of *Ku80*, *p53*, or other DNA damage response genes (Figures S3A–S3D). These results further support the notion that TopoII is a novel parallel pathway independent of DNA damage repair pathways mediating poly(GR) toxicity in *Drosophila* (Figure S3E).

To examine whether TopoII modifies *C9ORF72*-related neurodegeneration in human ALS/FTD patient neurons, we used an ASOs to partially knockdown *TopoIIβ* expression in control human motor neurons (Figure 3F). Unlike *TopoIIα*, *TopoIIβ* is highly expressed in mammalian postmitotic neurons and has a key role in the transcriptional regulation of neuronal immediate-early genes and neuronal survival[36,37]. As reported before[33], *C9ORF72*-ALS patient motor neurons were more vulnerable than control neurons upon withdrawal of neurotrophic factors (Figure 3G). Interestingly, partial downregulation of *TopoIIβ* by two different ASOs significantly increased the survival of *C9ORF72*-ALS patient motor neurons (Figure 3H) but had no effect in controls (3 donors per genotype, Figure 3I). Thus, upregulation of *TopoIIβ* also contributes to neurodegeneration in *C9ORF72* patient neurons.

Upregulation of Mtk and Hsp90 in Poly(GR)-expressing Flies Is Controlled by Topoisomerase II

It is not known how Mtk and Hsp90 expression levels are upregulated during poly(GR)-induced neurodegeneration. We found that the level of TopoII was increased in poly(GR)-expressing flies. This observation was made at the mRNA level by RT-qPCR analysis (Figure 4A), protein levels as measured by western blot analysis (Figures 4B and 4C), and immunostaining (Figure S4A). In *C9ORF72* iPSC-derived motor neurons, TopoIIβ protein levels were elevated (Figures 4D and 4E), similar to that in our *Drosophila* model (Figures 4B, 4C).

Because TopoII is also a genetic modifier of poly(GR) toxicity, we investigated whether TopoII regulates Mtk activation in poly(GR)-expressing flies. To this end, we used two different *TopoII*-specific RNAi lines to decrease *TopoII* mRNA expression level in poly(GR)-expressing flies to the level in control flies (Figure 4F). This manipulation greatly attenuated the increased expression of the *AMP* gene *Mtk* (Figure 4G), but not of *DptB* (Figure 4H). The effects of TopoII downregulation on Mtk expression were not due to changes in poly(GR) level, as *poly(GR)* mRNA and protein levels were not regulated by TopoII (Figure 4I, 4J). Thus, upregulation of the AMP gene *Mtk* in response to poly(GR) toxicity is mediated in part through transcriptional regulation by TopoII. Poly(GR) expression increased *Hsp90* mRNA expression and partial knockdown of *TopoII* by two different RNAi lines restored the *Hsp90* mRNA level to that of control flies (Figure 4K) but did not affect some other heat shock pathway genes such as *Hsp27* (Figure 4L), *Hsp23* (Figure S4B), *Hsp68* (Figure S4C), and *Hsf* (Figure S4D). Moreover, we performed a chromatin immunoprecipitation (ChIP) experiment in HEK293T cells and demonstrated that *TopoIIβ* directly binds to the promotor region of the *HSP90AA1* gene (Figures 4M and 4N). Thus, poly(GR)-induced overactivation of Hsp90 is mediated by transcriptional regulation of TopoII, revealing a direct regulatory link between TopoII and Hsp90 in *C9ORF72*-related neurodegeneration.

DISCUSSION

Using *Drosophila* as an experimental system, we identified the AMP gene *Mtk* as a novel genetic modifier of poly(GR) toxicity in *C9ORF72*-related neurodegeneration. The Mtk level was greatly elevated in poly(GR)-expressing flies, and downregulation of Mtk suppressed poly(GR) toxicity, highlighting the role of overactivated Mtk in poly(GR)-induced neurotoxicity. In our study, neuron-specific knockdown of *Mtk* could partially rescue poly(GR)-induced climbing defects while *Mtk* overexpression in neurons had the opposite effect (Figure 1J), indicating that Mtk has a cell-autonomous role in promoting neurodegeneration. Whether overactivation of Mtk in glial cells also contributes to poly(GR)-induced neurotoxicity remains to be investigated. Mtk is one of many innate immunity–related AMPs that protect insects against invading bacteria, fungi, and other pathogens[27]. Different AMPs have remarkable specificity targeting diverse pathogens[38]. However, their endogenous functions in the nervous system during development or aging are poorly understood. Some AMPs are involved in dendrite degeneration during aging and infection in *C. elegans*[39] and in neuronal cell loss after traumatic brain injury in

*Drosophila*40. Our findings here provide the first example that activation of the AMP gene *Mtk* has a cell-autonomous role in promoting neurodegeneration caused by FTD/ALS-related disease proteins. *AMP* genes are present in mammals but their encoded amino acid sequences differ from those in insects[27]. In addition, mammals have evolved with highly complex innate immune systems[41]. It remains to be determined which specific AMPs and related molecular pathways in human neurons or glial cells contribute to *C9ORF72*-related neurodegeneration. Moreover, loss of C9ORF72 protein function may alter immune cell function[42]. It will be interesting to investigate how poly(GR) and partial loss of C9ORF72 synergize to dysregulate the *AMP* gene pathway in neurons and glial cells.

In identifying upstream regulators of the AMP gene *Mtk*, we found that downregulation of Hsp90 also suppressed poly(GR)-induced neurotoxicity without affecting poly(GR) level in *Drosophila*. This suppressor effect correlates with attenuated poly(GR)-induced Mtk activation. However, the molecular link between Hsp90 and Mtk is unclear, which is a limitation of our study. It is possible that under pathological conditions, elevated Hsp90 may participate in the regulatory circuit that activates *Mtk* expression. Indeed, some Hsp90-ligand complexes can activate innate immunity in certain cell types[43,44]. Alternatively, downregulation of Hsp90 may indirectly affect Mtk activation through attenuated poly(GR) toxicity. It remained to be determined how Hsp90 in poly(GR)-expressing cells activates Mtk or other genes in the innate immunity pathway. More importantly, knockdown of *HSP90AA1* expression also partially rescued neurodegeneration in *C9ORF72* iPSC-derived motor neurons, revealing an unexpected role for Hsp90 in promoting *C9ORF72*-related neurodegeneration. Our results are consistent with the work by Mordes *et al.*[31] who reported that HSF1, the master transcription factor that controls the expression of many heat shock proteins, is upregulated in both poly(GR)-expressing flies and *C9OAF72*-ALS/FTD patient brains and contributes to poly(GR) toxicity[31]. However, this study did not specifically examine the role of Hsp90, thus, our work extended their findings and pinpointed Hsp90, the most abundant constitutively expressed stress protein in the cell[28,29], as a key player in the upregulation of antimicrobial peptides and potentially activation of other innate immune responses that further exacerbate neurodegenerative processes. Moreover, our ChIP analysis indicates that *HSP90AA1* expression is directly regulated by TopoIIβ, and downregulation of TopoIIβ also partially suppresses neurodegeneration in *C9ORF72* iPSC-derived motor neurons. Thus, the TopoII-regulated Hsp90 and some AMPs are novel modifier genes in *C9OAF72*-ALS/FTD related neurodegeneration and downregulation of these genes represents a potential therapeutic avenue.

STAR★METHODS

RESOURCE AVAILABILITY

Lead contact—Further information and requests for resources and reagents should be directed to and will be fulfilled by the lead contact, Fen-Biao Gao (fen-biao.gao@umassmed.edu)

Materials availability—Requests for resources and additional information should be directed to and will be fulfilled by the lead contact. Reagents generated in this study will be

made available on request, but we may require a completed Materials Transfer Agreement if there is potential for commercial application.

Data and code availability—All data are available in the main text or supplementary materials and will be shared by the lead contact upon request. Any additional information required to reanalyze the data reported in this work paper is available from the Lead Contact upon request.

EXPERIMENTAL MODEL DETAILS

***Drosophila* strains and genetics—**Flies were maintained at 25°C on a standard yeast diet unless otherwise stated. *GMR-Gal4* (BL9146), *elav-Gal4* (BL8765), *Tub-Gal80^{ts}* (BL7019), *UAS-GFP, UAS-mCherry RNAi* (BL35785) *w^{1118}* (BL3605), *UAS-Mtk RNAi-1* (v8792), *UAS-Mtk RNAi-2* (v109740), *UAS-Mtk RNAi-3* (BL28546), *UAS-Hsp23 RNAi-1* (BL82961), *UAS-Hsp23 RNAi-2* (BL44029), *UAS-Hsp26 RNAi*-1 (v100955), *UAS-Hsp26 RNAi-2* (BL35408), *UAS-Hsp27 RNAi*-1 (BL33007), *UAS-Hsp27 RNAi*-2 (BL33922), *UAS-Hsp70 RNAi* (BL35671), *UAS-Hsp90 RNAi* (BL33947), *UAS-Hsp90* (BL58469), *Hsp90^{e6A}* (BL36576), *Hsp90^{e6D}* (BL5696), *Hsf^{1}* (BL5491), *UAS-TopoII RNAi-1* (BL31342), *UAS-TopoII RNAi-2* (BL35416) mutant and RNAi lines were from the Bloomington *Drosophila* Stock Center and the Vienna *Drosophila* Resource Center. *Dpt^{SK1}* and *Mtk^{R1}* mutant lines were kindly provided by Dr. Bruno Lemaitre (Ecole Polytechnique of Lausanne, Switzerland). The *Dpt^{SK1}* line includes two deletions removing both *DptA* and *DptB* genes. *UAS-Mtk* line was gift from by Dr. Stanislava Chtarbanova (University of Alabama). *GMR-Gal4*, *Tub-GAL80^{ts}*, *UAS-(GR)$_{80}$/CyO* and *Elav-Gal4*, *Tub-Gal80^{ts}/CyO*; *UAS-Control-(GR)$_{80}$/TM6B*, *Tb*, and *Elav-Gal4*, *Tub-Gal80^{ts}*, *UAS-(GR)$_{80}$/CyO* lines were generated in our laboratory[22,24]. All the fly genotypes in this study is in Table S1.

Human iPSC culture—We used previously published iPSC lines from two *C9ORF72* carriers (26L6 and 27L11) and its isogenic control lines (26Z90 and 27M91) with CRISPR/Cas9-mediated deletion of expanded G_4C_2 repeats[22]. The use of these human iPSC lines is approved by UMass Chan Medical School Institutional Biosafety Committee (Docket # I-435-20). Briefly, iPSCs were plated and expanded in mTSER1 medium (mTeSR™1 5X Supplement diluted 1:5 in mTeSR™1 Basal Medium, Stem Cell Technologies) on coated 6-well plates with Matrigel diluted 1:100 in Knockout DMEM (GIBCO/Thermo Fisher Scientific). The mTSER1 medium was replaced every day. When cells reach 70-80% confluent, wash with DPBS and dissociate with accutase (Millipore) diluted 1:3 in DPBS. After washing with DPBS, cells were scraped with a cell lifter in mTSER1 medium and seeding into Matrigel-coated plates at the desired number. The mTSER1 medium was replaced every day and remove differentiating cells/colonies if necessary.

Motor neuron differentiation for western blot—Human iPSCs were differentiated in motor neurons with some modifications as described[22]. Briefly, iPSCs were expanded in Matrigel-coated wells and at 60% confluency were split with accutase (Millipore) into Matrigel-coated wells; 24 h after plating, the culture medium was replaced with neuroepithelial progenitor (NEP) medium, including DMEM/F12 (Gibco), Neurobasal medium (Gibco) at 1:1, 0.5X N2 supplement (Gibco), 0.5X B27 supplement (Gibco),

0.1 mM ascorbic acid (Sigma), 1X Glutamax (Invitrogen), 3 μM CHIR99021 (Tocris Bioscience), 2 μM DMH1 (Tocris Bioscience), and 2 μM SB431542 (Stemgent), for 6 days. NEPs were dissociated with accutase and split 1:6 into Matrigel-coated wells. NEPs were cultured in motor neuron progenitor (MNP) induction medium (the same NEP medium as described above with 0.1 μM retinoic acid (Stemgent) and 0.5 μM Purmorphamine (Stemgent) for 6 days. MNPs were dissociated with accutase and split into culture dishes (Corning) to generate suspension cultures. The cells were cultured in motor neuron differentiation medium (the same NEP medium as described above with 0.5 μM retinoic acid and 0.1 μM Purmorphamine) for 6 days. Lastly, the cells were dissociated into single cells, plated on laminin-coated plates/coverslips in motor neuron media, including Neurobasal medium, 0.5X B27 supplement, 0.1 mM ascorbic acid, 1X Glutamax, 0.1 μM Compound E (Calbiochem), 0.26 μg/ml cAMP, 1 μg/ml Laminin (Sigma), 10 ng/ml GDNF (R&D Systems), and 10 ng/ml GDNF (R&D Systems), and 10 ng/ml BDNF, for up to 3 months.

Generating induced motor neurons for survival—Induced motor neurons (iMNs) were generated as described[33]. Cells were purchased from Coriell Institute. The control lines were ND03231 (CTRL-1), ND03719 (CTRL-2), and ND05280 (CTRL-3). The *C9ORF72*-ALS lines were ND06769 (C9 ALS-1), ND10689 (C9 ALS-2), and ND12099 (C9 ALS-3). Briefly, human secondary fibroblasts were transduced with a cocktail of transcription factors (*Ascl1*, *Brn2*, *Isl1*, *Lhx3*, *Ngn2*, *NeuroD1*, and *Mytl1*) using retrovirus. The next day, Hb9::RFP^{+} lentivirus was added to the fibroblast cultures. On Day 4, primary glia isolated from male and female ICR mouse pups (P2–P3) were added to the cultures in glia medium. To induce the formation of neurons, the medium was replaced the following day with N3 medium consisting of DMEM/F-12 (Life Technologies), 2% fetal bovine serum, B-27 and N2 supplements (Life Technologies), 1% penicillin/streptomycin, 7.5 μM Rep Sox (Selleck), and growth factors (GDNF, BDNF, CNTF, and FGF, 10 ng/ml each, R&D Systems). The culture medium was fully replenished every 2 days, until 14 days after transduction.

METHOD DETAILS

RNA-seq—Total RNA from heads of 3-week-old control and $(GR)_{80}$ male flies aged at 25 °C was isolated with the Qiagen miRNeasy Kit (Qiagen, catalog no. 217604). RNA-seq libraries were prepared with the Ovation Universal RNA-seq system and *Drosophila* rRNA depletion module according to the manufacturer's protocol (Nugen, catalog no. 0343). cDNA was fragmented with an ultrasonicator (catalog no. E220, Covaris). Library size distribution was assessed with on Agilent Bioanalyzer. Libraries were sequenced with an Illumina HiSEq Platform PE 150.

RNA-seq analysis—Sequenced reads were trimmed for Illumina adaptors and low-quality bases with Trimmomatic (v0.39)[45] and aligned to the dm6 genome with HISAT2 (v2.2.1)[46]. Read counts per gene were calculated with HTSeq[47] and FlyBase gene annotations (dmel-all-r6.34.mod.gtf)[48]. Differential gene expression was analyzed with DESeq2. Gene Ontology analysis was done with PantherDB[49], and protein–protein network analysis was done with STRING[50]. Relevant code for this analysis can be found at https://github.com/weng-lab/Fly-ALS-Project.

RNA extraction and real-time quantitative PCR—Fly heads were collected and frozen in liquid nitrogen. Total RNA was extracted with QIAzol and the RNeasy Mini Kit (catalog no. 74106, Qiagen), and 1 μg of RNA of each sample was then reverse transcribed to cDNA with the TaqMan Reverse Transcription Kit (catalog no. N8080234, Thermo Fisher Scientific). Real-time quantitative PCR (RT-qPCR) was done with SYBR Select Master Mix (catalog no. 4472918, Thermo Fisher Scientific) on a QuantStudio 3 System. Ct values for each gene were normalized to internal controls as indicated. Relative mRNA expression was calculated with the 'delta-delta Ct' method.

Total RNA from iPSC-derived motor neurons was extracted with the RNeasy Plus Mini Kit (Qiagen) 72 h after ASO administration and reverse transcribed with an Oligo-dT and a Protoscript II First Strand Synthesis Kit (NEB). RNA integrity was assessed with a NanoDrop 1000 (Thermo). RT-qPCR was performed with an Applied Biosystems ViiA 7 Real-Time PCR System (Life Technologies) and iTaq Universal SYBR Green Supermix (Bio-Rad). Gene expression levels were normalized to the mRNA levels of *GAPDH* or *HPRT*. All the primer information is in Table S2.

Quantification of *Drosophila* external eye phenotype—All flies for eye phenotype analysis were crossed and raised at 23 °C to avoid lethality. Flies were collected and aged for ~10 days to see degenerative eye phenotype. Eye phenotypes of 10-day-old adult flies were immobilized by freezing at −20°C for 4 hr, and then imaged under a dissecting microscope (Nikon, SMZ 1500). To quantify the phenotypical differences between adult eyes in each genotype, we use an eye phenotype grading scale as a relative output of how much a gene or treatment modifies the ommatidia while toxic poly(GR) is expressed in the eye. Phenotype categories correspond to the levels of eye degeneration observed and are classified into the following 4 groups. (1) Absent: wild-type, driver-only transgenic flies were used as the baseline to establish this phenotype. All ommatidia are completely normal, well organized, have normal pigment, and show no disruptions. (2) Weak: ommatidia are slightly abnormal in size and arrangement of cells, there is a partial loss of pigment, but no necrosis (black tissue) is observed. (3) Medium: there is considerable disarrangement to the ommatidia and their size, more cells have loss of pigment, and there is obvious necrosis in the eye. (4) Severe: substantial necrosis and loss of ommatidia in the eye, leading to a noticeably smaller eye size. Each group of flies was quantified by category, and the data were analyzed by chi-square test.

***Drosophila* eye internal section with TB staining—**Flies reared at 23°C and aged for ~10 days and then were anesthetized with CO_2. Fly heads were hemisected, and fixed overnight at 4°C in 0.05 M Sodium Cacodylate buffer containing 2.5% Glutaraldehyde. The samples were then washed with the buffer solution three times, and fixed again with 2% Osmium tetroxide for 2 hr. After rinse with D.W, the samples were then dehydrated through an ethanol series (10%, 30%, 50%, 70%, 85%, 95%, and 100%), and the head tissues were incubated in 100% propylene oxide for 1 h at room temperature. The samples were transferred to 1:1 ratio of Poly/Bed and propylene oxide at room temperature for overnight, and then embedded in Poly/Bed 812 resin. Eye cross-sections were cut either at 1 μM

thickness and stained with 1% toluidine blue (TB) for confocal microscopy in bright-filed (Carl Zeiss, LSM800).

Negative geotaxis climbing assay—All the flies were crossed and raised at 18°C until eclosion to avoid developmental defects. Twenty male flies were collected and maintained at 27°C for 3 weeks. For climbing assay, aged flies were placed in a 10 cm long plastic vial and incubated for 3 h at room temperature for environmental adaptation. Using negative geotaxis in *Drosophila*, we tapped to the bottom of the vial and counted the number of flies that climbed 3 cm in 5 sec. The assay was repeated twice for each vial. For each genotype, at least total of 100 flies were analyzed.

Poly(GR) measurement—RIPA buffer soluble and urea buffer extracted poly(GR) levels in flies were measured with a Meso Scale Discovery (MSD)-based immunoassay and custom-made polyclonal anti-poly(GR) antibodies as described (Yuva-Aydemir Y et al., 2019). Briefly, 30-40 frozen aged fly heads were lysed, and diluted to the same concentration, and tested in duplicate wells. Response values upon electrochemical stimulation were acquired with a plate reader (QuickPlex SQ120, Meso Scale Discovery). All response signals were background corrected and interpolated against standard curve using $(GR)_8$ peptide and presented as concentration in ng/mg units.

Western blot analysis—Motor neurons were briefly washed with PBS and homogenized in RIPA buffer (Thermo Scientific, 89901) containing protease and phosphatase inhibitor Cocktail (catalog no. 5872, Cell Signaling) and the lysates were centrifuged at 14,000 × g for 15 min at 4°C to remove the debris. The supernatant was transferred and quantified with a Pierce BCA protein assay (Thermo Scientific, 23227) The lysates were mixed with 4× Laemmli Sample Buffer (Bio-Rad, 1610747) with beta-mercaptoethanol (Sigma, M3148-100ML) and incubated for 10 min at 95 °C for 10 min. Adult fly heads were homogenized in 2× Laemmli buffer (catalog no. 1610737, Bio-Rad) containing beta-mercaptoethanol (Sigma, M3148-100ML) and protease and phosphatase inhibitor Cocktail (catalog no. 5872, Cell Signaling). Lysates were incubated at 95 °C for 5 min and centrifuged for 5 min at 16,000 × g to remove the debris. Proper amounts of lysates were separated by SDS-PAGE and immunoblotted with rabbit anti-TopoIIβ (1:2,000; NBP1-89527, Novus), mouse anti-HSP90 (1:2,000; Cat# 610419, BD Biosciences), mouse anti β-actin (1: 2,000, Cat# sc-47778, Santa Cruz Biotechnology), rabbit anti-TopoII (1:5,000; a gift from Dr. Donna Arndt-Jovin, Max Planck Institute for Biophysical Chemistry), or mouse anti-actin (1: 2,000; JLA20, Developmental Studies Hybridoma Bank) overnight at 4 °C, and transferred to PVDF membranes. After washing with 1x TBST, the membranes were incubated with IRDye 680RD goat anti-rabbit (catalog no. 926-68071, LI-COR Biosciences) or IRDye 800RD donkey anti-mouse (catalog no. 926-32212, LI-COR Biosciences) secondary antibodies. All blocking and antibody dilutions were done with Odyssey Blocking Buffer (catalog no. 927-40010, LI-COR Biosciences).

Drug administration for *Drosophila*—For drug treatment experiments, fly embryos were raised in plastic vials with instant medium (catalog no. 173202, Carolina Biological Supply) containing vehicle or 1.0 or 10 μM doxorubicin (catalog no. D1515, Sigma-Aldrich)

dissolved in water. Flies were grown on food containing vehicle or doxorubicin at 23 °C and collected for analysis at 3 days of age.

Immunohistochemistry—Third instar larval brains were dissected in phosphate-buffered saline (PBS), fixed in 4% paraformaldehyde for 4 min, and washed three times with PBS containing 0.1% Triton X-100 (PBST). Larval tissues were blocked with 2% normal goat serum in PBST and incubated with rabbit anti-TopoII (1:1000; a gift from Dr. Donna Arndt-Jovin, Max Planck Institute for Biophysical Chemistry) primary antibody for overnight at 4 °C. The samples were washed three times with PBST and incubated with donkey anti-rabbit Alexa Fluor 568 secondary antibody (catalog no. A10042, Thermo Scientific) and Hoechst 33258 (1:1000; catalog no. H3569, Fisher Scientific) for 1 h at room temperature. After three washes with PBST, larval brains were dissected and mounted with Vectashield mounting medium (Vector Laboratories).

Chromatin immunoprecipitation (ChIP) assay—ChIP assays were performed using ChIP Kit (Abcam, ab500) following the manufacturer's protocol with some modifications (Liu et al., 2017). Briefly, 3xFlag or 3xFlag-TopoIIβ expressing HEK293T cells were treated with the fresh fixing buffer (1.1% formaldehyde in PBS) at room temperature for 10 minutes for the crosslinking of DNA and proteins. The reaction was stopped with the glycine buffer provided in the kit, and cells were pelleted by centrifugation at 500 × g for 5 minutes at 4°C. Cells were then lysed and the chromatin was sheared by sonication to about 200-1,000 base pairs in length at 30% amplitude for 15 min with 10 sec pulse on and 50 sec pulse off time using Fisherbrand™ Model 120 Sonic Dismembrator (Fisher Scientific, FB120110). The DNA fragments were then immunoprecipitated with antibodies against Flag (Sigma-Aldrich, M8823) for 2 hr and were purified with DNA purifying slurry provided in the kit. The immunoprecipitated DNA fragments and input DNA were amplified by PCR using specific primers targeting the amplicons of *HSP90AA1* DNA sequence. PCR products were analyzed on a 2% agarose gel. The following primers were used for amplifying the amplicon 1 (forward: 5'-gttcgggaggcttctggaaa-3' and reverse primer 5'-gggacgctgaagcaactga-3'), amplicon 2 (forward: 5'-aatggcagaaactgcggtag-3' and reverse primer 5'-ctttgcctgtttccttcctg-3'), and amplicon 3 (forward: 5'-acattaaagatggggcctga-3' and reverse primer 5'-ctttgttttggggaccttca-3'). All the experiments were repeated at least three times.

Neuron survival assay and ASO treatment—Neuronal survival was assayed starting on Day 14, when the iMNs were maintained in N3 medium without neurotrophic factors or RepSox. Baseline images were taken using the Molecular Devices Image Express prior to the addition of antisense oligonucleotide (ASO)s. The following day iMNs were treated (a single time) with 9 μM of negative control ASO, *HSP90AA1* ASOs, or *TopoIIβ* ASOs for 72 h. The ASOs were synthesized by Integrated DNA Technologies which contained phosphorothioate bonds and the modified base 2'-O-methoxy-ethyl (MOE) for increased stability and binding affinity to the mRNA target of interest. For longitudinal tracking of Hb9::RFP iMNs, the plates were imaged every 2 days, and iMNs were manually counted with SVCell 3.0 (DRVision Technologies). Neurons were scored as dead when their soma were no longer visible.

ASOs used for iMN survival experiment—For *HSP90AA1* experiments, the negative control ASO was mG*mC*mG*mA*mC*T*A*T*A*C*G*C*G*C*A*mA*mU*mA*mU*mG, *HSP90AA1* ASO-1 was mU*mU*mU*mU*mC*T*T*C*A*G*C*C*T*C*A*mU*mC*mA*mU*mC and *HSP90AA1* ASO-2 was mC*mC*mU*mC*mA*G*C*C*A*G*A*G*A*T*T*mA*mG*mU* mC*mU. For *TopoIIβ* experiments, the *TopoIIβ* ASO-1 was eA*eG*eC*eA*eG*G*T*C*T*G*T*A*G*T*T*eT*eG*eT*eA*eA and ASO-2 eG*eA*eA*eT*eG*T*C*T*T*G*C*A*C*A*G*eT*eT*eT*eC*eA. *= phosphorothioate linkage, m = 2'-O-methyl ribose, e = 2'-O-methoxyethyl ribose.

QUANRIFICATION AND STATISTICAL ANALYSIS

Statistical analysis—Data were analyzed and graphs were made with Prism (GraphPad). For comparisons of different treatment groups or genotypes, two-tailed unpaired *t* tests were used for two groups and a one-way ANOVA followed by a Tukey' s or Dunnett's post hoc analysis was used for more than two groups. Categorical data were analyzed by chi-square test. Statistical analysis of iMN survival experiments was conducted a two-sided log-rank test. Data are presented as mean ± s.e.m. $P<0.05$ was considered statistically significant. Statistical analysis of RNA-seq data and Gene Ontology is described in RNA Seq and Gene Ontology analysis above.

Supplementary Material

Refer to Web version on PubMed Central for supplementary material.

ACKNOWLEDGEMENTS

We thank the Bloomington *Drosophila* Stock Center, the Vienna *Drosophila* Resource Center, Dr. Bruno Lemaitre and Dr. Stanislava Chtarbanova for fly lines, Dr. Donna Arndt-ovin for TopoII antibody, the NINDS Biorepository for providing several cell lines used for this study, and Dr. Hong-Sheng Li and the UMass Chan Medical School Electron Microscopy Core for help with fly eye sectioning. We also thank anonymous reviewers for constructive suggestions. This work was supported by grants from the NIH (R37NS057553 and R01NS101986 to F.-B.G., R01AI060025 to N.S., HG012343 to Z.W., R01NS097850 and R44NS097094 to J.K.I.), the Target ALS Foundation (F.-B.G.), and the Association for Frontotemporal Degeneration (F.-B.G. and J.K.I.), and the Korean National Center for Research Resources (SI0OD21580 to Y.-W.J.). J.K.I. is also supported by US Department of Defense grants W81XWH-20-1-0424, W81XWH-21-1-0168, and W81XWH-21-1-0131 and by grants from the Tau Consortium, the New York Stem Cell Foundation, the Alzheimer's Drug Discovery Foundation, the John Douglas French Alzheimer's Foundation, and the Merkin Family Foundation. J.K.I. is a New York Stem Cell Foundation-Robertson Investigator and the John Douglas French Alzheimer's Foundation Endowed Professor of Stem Cell Biology and Regenerative Medicine. G.R.L. was supported in part by a Broad Postdoctoral Fellowship.

DECLARATION OF INTERESTS

F.-B.G. has an active research agreement with and receives funding from Stealth BioTherapeutics. Z. W. co-founded Rgenta Therapeutics, and she serves as a scientific advisor for the company and is a member of its board. J.K.I. is a co-founder of AcuraStem, Inc. and Modulo Bio, serves on the scientific advisory boards of AcuraStem, Spinogenix, Synapticure, and Vesalius Therapeutics, and is employed at BioMarin Pharmaceutical.

REFERENCES

1. DeJesus-Hernandez M, Mackenzie IR, Boeve BF, Boxer AL, Baker M, Rutherford NJ, Nicholson AM, Finch NA, Flynn H, Adamson J, et al. (2011). Expanded GGGGCC hexanucleotide repeat in

noncoding region of C9ORF72 causes chromosome 9p-linked FTD and ALS. Neuron 72, 245–256. 10.1016/j.neuron.2011.09.011. [PubMed: 21944778]

2. Renton AE, Majounie E, Waite A, Simón-Sánchez J, Rollinson S, Gibbs JR, Schymick JC, Laaksovirta H, van Swieten JC, Myllykangas L, et al. (2011). A hexanucleotide repeat expansion in C9ORF72 is the cause of chromosome 9p21-linked ALS-FTD. Neuron 72, 257–268. 10.1016/j.neuron.2011.09.010. [PubMed: 21944779]
3. Ash PE, Bieniek KF, Gendron TF, Caulfield T, Lin WL, Dejesus-Hernandez M, van Blitterswijk MM, Jansen-West K, Paul JW 3rd, Rademakers R, et al. (2013). Unconventional translation of C9ORF72 GGGGCC expansion generates insoluble polypeptides specific to c9FTD/ALS. Neuron 77, 639–646. 10.1016/j.neuron.2013.02.004. [PubMed: 23415312]
4. Mori K, Weng SM, Arzberger T, May S, Rentzsch K, Kremmer E, Schmid B, Kretzschmar HA, Cruts M, Van Broeckhoven C, et al. (2013). The C9orf72 GGGGCC repeat is translated into aggregating dipeptide-repeat proteins in FTLD/ALS. Science 339, 1335–1338. 10.1126/science.1232927. [PubMed: 23393093]
5. Zu T, Liu Y, Bañez-Coronel M, Reid T, Pletnikova O, Lewis J, Miller TM, Harms MB, Falchook AE, Subramony SH, et al. (2013). RAN proteins and RNA foci from antisense transcripts in C9ORF72 ALS and frontotemporal dementia. Proc. Natl. Acad. Sci. USA 110, 4968–4977. 10.1073/pnas.1315438110. [PubMed: 23479608]
6. Saberi S, Stauffer JE, Jiang J, Garcia SD, Taylor AE, Schulte D, Ohkubo T, Schloffman CL, Maldonado M, Baughn M, et al. (2018). Sense-encoded poly-GR dipeptide repeat proteins correlate to neurodegeneration and uniquely co-localize with TDP-43 in dendrites of repeat-expanded C9orf72 amyotrophic lateral sclerosis. Acta Neuropathol. 135, 459–474. 10.1007/s00401-017-1793-8. [PubMed: 29196813]
7. Sakae N, Bieniek KF, Zhang YJ, Ross K, Gendron TF, Murray ME, Rademakers R, Petrucelli L, and Dickson DW (2018). Poly-GR dipeptide repeat polymers correlate with neurodegeneration and Clinicopathological subtypes in C9ORF72-related brain disease. Acta Neuropathol. Commun 6, 63. 10.1186/s40478-018-0564-7. [PubMed: 30029693]
8. Quaegebeur A, Glaria I, Lashley T, and Isaacs AM (2020). Soluble and insoluble dipeptide repeat protein measurements in C9orf72-frontotemporal dementia brains show regional differential solubility and correlation of poly-GR with clinical severity. Acta Neuropathol. Commun 8, 184. 10.1186/s40478-020-01036-y. [PubMed: 33168090]
9. Gitler AD, and Tsuiji H (2016). There has been an awakening: Emerging mechanisms of C9orf72 mutations in FTD/ALS. Brain Res 1647, 19–29. 10.1016/j.brainres.2016.04.004. [PubMed: 27059391]
10. Gao FB, Almeida S, and Lopez-Gonzalez R (2017). Dysregulated molecular pathways in amyotrophic lateral sclerosis-frontotemporal dementia spectrum disorder. EMBO J 36, 2931–2950. 10.15252/embj.201797568. [PubMed: 28916614]
11. Schmitz A, Pinheiro Marques J, Oertig I, Maharjan N, and Saxena S (2021). Emerging perspectives on dipeptide repeat proteins in C9ORF72 ALS/FTD. Front. Cell. Neurosci 15, 637548. 10.3389/fncel.2021.637548. [PubMed: 33679328]
12. Freibaum BD, Lu Y, Lopez-Gonzalez R, Kim NC, Almeida S, Lee KH, Badders N, Valentine M, Miller BL, Wong PC, et al. (2015). GGGGCC repeat expansion in C9orf72 compromises nucleocytoplasmic transport. Nature 525, 129–133. 10.1038/naturel4974. [PubMed: 26308899]
13. Jovičić A, Mertens J, Boeynaems S, Bogaert E, Chai N, Yamada SB, Paul JW 3rd, Sun S, Herdy JR, Bieri G, et al. (2015). Modifiers of C9orf72 dipeptide repeat toxicity connect nucleocytoplasmic transport defects to FTD/ALS. Nature neuroscience 18, 1226–1229. 10.1038/nn.4085. [PubMed: 26308983]
14. Zhang K, Donnelly CJ, Haeusler AR, Grima JC, Machamer JB, Steinwald P, Daley EL, Miller SJ, Cunningham KM, Vidensky S, et al. (2015). The C9orf72 repeat expansion disrupts nucleocytoplasmic transport. Nature 525, 56–61. 10.1038/nature14973. [PubMed: 26308891]
15. Boeynaems S, Bogaert E, Van Damme P, and Van Den Bosch L (2016). Inside out: the role of nucleocytoplasmic transport in ALS and FTLD. Acta Neuropathol. 132, 159–173. 10.1007/s00401-016-1586-5. [PubMed: 27271576]
16. Fumagalli L, Young FL, Boeynaems S, De Decker M, Mehta AR, Swijsen A, Fazal R, Guo W, Moisse M, Beckers J, et al. (2021). C9orf72-derived arginine-containing dipeptide repeats

associate with axonal transport machinery and impede microtubule-based motility. Science advances 7. 10.1126/sciadv.abg3013.

17. Kanekura K, Yagi T, Cammack AJ, Mahadevan J, Kuroda M, Harms MB, Miller TM, and Urano F (2016). Poly-dipeptides encoded by the C9ORF72 repeats block global protein translation. Hum. Mol. Genet 25, 1803–1813. 10.1093/hmg/ddw052. [PubMed: 26931465]
18. Lopez-Gonzalez R, Lu Y, Gendron TF, Karydas A, Tran H, Yang D, Petrucelli L, Miller BL, Almeida S, and Gao FB (2016). Poly(GR) in C9ORF72-related ALS/FTD compromises mitochondrial function and increases oxidative stress and DNA damage in iPSC-derived motor neurons. Neuron 92, 383–391. 10.1016/j.neuron.2016.09.015. [PubMed: 27720481]
19. Loveland AB, Svidritskiy E, Susorov D, Lee S, Park A, Zvornicanin S, Demo G, Gao FB, and Korostelev AA (2022). Ribosome inhibition by C9ORF72-ALS/FTD-associated poly-PR and poly-GR proteins revealed by cryo-EM. Nat. Commun 13, 2776. 10.1038/s41467-022-30418-0. [PubMed: 35589706]
20. Zhang YJ, Gendron TF, Ebbert MTW, O'Raw AD, Yue M, Jansen-West K, Zhang X, Prudencio M, Chew J, Cook CN, et al. (2018). Poly(GR) impairs protein translation and stress granule dynamics in C9orf72-associated frontotemporal dementia and amyotrophic lateral sclerosis. Nat. Med 24, 1136–1142. 10.1038/s41591-018-0071-1. [PubMed: 29942091]
21. Maor-Nof M, Shipony Z, Lopez-Gonzalez R, Nakayama L, Zhang YJ, Couthouis J, Blum JA, Castruita PA, Linares GR, Ruan K, et al. (2021). p53 is a central regulator driving neurodegeneration caused by C9orf72 poly(PR). Cell 184, 689–708.e620. 10.1016/j.cell.2020.12.025. [PubMed: 33482083]
22. Lopez-Gonzalez R, Yang D, Pribadi M, Kim TS, Krishnan G, Choi SY, Lee S, Coppola G, and Gao FB (2019). Partial inhibition of the overactivated Ku80-dependent DNA repair pathway rescues neurodegeneration in C9ORF72-ALS/FTD. Proc. Natl. Acad. Sci. USA 116, 9628–9633. 10.1073/pnas.1901313116. [PubMed: 31019093]
23. McGurk L, Berson A, and Bonini NM (2015). Drosophila as an in vivo model for human neurodegenerative disease. Genetics 201, 377–402. 10.1534/genetics.115.179457. [PubMed: 26447127]
24. Yuva-Aydemir Y, Almeida S, Krishnan G, Gendron TF, and Gao FB (2019). Transcription elongation factor AFF2/FMR2 regulates expression of expanded GGGGCC repeat-containing C9ORF72 allele in ALS/FTD. Nat. Commun 10, 5466. 10.1038/s41467-019-13477-8. [PubMed: 31784536]
25. Yang D, Abdallah A, Li Z, Lu Y, Almeida S, and Gao FB (2015). FTD/ALS-associated poly(GR) protein impairs the Notch pathway and is recruited by poly(GA) into cytoplasmic inclusions. Acta Neuropathol. 130, 525–535. 10.1007/s00401-015-1448-6. [PubMed: 26031661]
26. Zhang LJ, and Gallo RL (2016). Antimicrobial peptides. Curr. Biol 26, 14–19. 10.1016/j.cub.2015.11.017. [PubMed: 26687626]
27. Haney EF, Mansour SC, and Hancock RE (2017). Antimicrobial peptides: an introduction. Methods Mol. Biol 1548, 3–22. 10.1007/978-1-4939-6737-7. [PubMed: 28013493]
28. Schopf FH, Biebl MM, and Buchner J (2017). The HSP90 chaperone machinery. Nature reviews. Molecular cell biology 18, 345–360. 10.1038/nrm.2017.20. [PubMed: 28429788]
29. Wiech H, Buchner J, Zimmermann R, and Jakob U (1992). Hsp90 chaperones protein folding in vitro. Nature 358, 169–170. 10.1038/358169a0. [PubMed: 1614549]
30. Kmiecik SW, and Mayer MP (2021). Molecular mechanisms of heat shock factor 1 regulation. Trends Biochem. Sci 47, 218–234. 10.1016/j.tibs.2021.10.004. [PubMed: 34810080]
31. Mordes DA, Prudencio M, Goodman LD, Klim JR, Moccia R, Limone F, Pietilainen O, Chowdhary K, Dickson DW, Rademakers R, et al. (2018). Dipeptide repeat proteins activate a heat shock response found in C9ORF72-ALS/FTLD patients. Acta Neuropathol. Commun 6, 55. 10.1186/s40478-018-0555-8. [PubMed: 29973287]
32. Choi SY, Lopez-Gonzalez R, Krishnan G, Phillips HL, Li AN, Seeley WW, Yao WD, Almeida S, and Gao FB (2019). C9ORF72-ALS/FTD-associated poly(GR) binds Atp5a1 and compromises mitochondrial function in vivo. Nature neuroscience 22, 851–862. 10.1038/s41593-019-0397-0. [PubMed: 31086314]

33. Shi Y, Lin S, Staats KA, Li Y, Chang WH, Hung ST, Hendricks E, Linares GR, Wang Y, Son EY, et al. (2018). Haploinsufficiency leads to neurodegeneration in C9ORF72 ALS/FTD human induced motor neurons. Nat. Med 24, 313–325. 10.1038/nm.4490. [PubMed: 29400714]
34. Nitiss JL (2009). DNA topoisomerase II and its growing repertoire of biological functions. Nat. Rev. Cancer 9, 327–337. 10.1038/nrc2608. [PubMed: 19377505]
35. Sritharan S, and Sivalingam N (2021). A comprehensive review on time-tested anticancer drug doxorubicin. Life Sci. 278, 119527. 10.1016/j.lfs.2021.119527. [PubMed: 33887349]
36. Madabhushi R, Gao F, Pfenning AR, Pan L, Yamakawa S, Seo J, Rueda R, Phan TX, Yamakawa H, Pao PC, et al. (2015). Activity-induced DNA breaks oovern the expression of neuronal aarly-response genes. Cell 161, 1592–1605. 10.1016/j.cell.2015.05.032. [PubMed: 26052046]
37. Tiwari VK, Burger L, Nikoletopoulou V, Deogracias R, Thakurela S, Wirbelauer C, Kaut J, Terranova R, Hoerner L, Mielke C, et al. (2012). Target genes of Topoisomerase IIβ regulate neuronal survival and are defined by their chromatin state. Proc. Natl. Acad. Sci. USA 109, 934–943. 10.1073/pnas.l119798109.
38. Hanson MA, Dostálová A, Ceroni C, Poidevin M, Kondo S, and Lemaitre B (2019). Synergy and remarkable specificity of antimicrobial peptides in vivo using a systematic knockout approach. eLife 8. 10.7554/eLife.44341.
39. E L, Zhou T, Koh S, Chuang M, Sharma R, Pujol N, Chisholm AD, Eroglu C, Matsunami H, and Yan D (2018). An antimicrobial peptide and its neuronal receptor regulate dendrite degeneration in aging and infection. Neuron 97, 125–138.e125. 10.1016/j.neuron.2017.12.001. [PubMed: 29301098]
40. Swanson LC, Rimkus SA, Ganetzky B, and Wassarman DA (2020). Loss of the antimicrobial peptide Metchnikowin protects against traumatic brain injury outcomes in Drosophila melanogaster. G3 10, 3109–3119. 10.1534/g3.120.401377. [PubMed: 32631949]
41. Riera Romo M, Pérez-Martínez D, and Castillo Ferrer C (2016). Innate immunity in vertebrates: an overview. Immunology 148, 125–139. 10.1111/imm.12597. [PubMed: 26878338]
42. Lall D, and Baloh RH (2017). Microglia and C9orf72 in neuroinflammation and ALS and frontotemporal dementia. J. Clin. Invest 127, 3250–3258. 10.1172/jci90607. [PubMed: 28737506]
43. Tamura Y, Yoneda A, Takei N, and Sawada K (2016). Spatiotemporal Regulation of Hsp90-Ligand Complex Leads to Immune Activation. Frontiers in immunology 7, 201. 10.3389/fimmu.2016.00201. [PubMed: 27252703]
44. Wallin RP, Lundqvist A, Moré SH, von Bonin A, Kiessling R, and Ljunggren HG (2002). Heat-shock proteins as activators of the innate immune system. Trends Immunol. 23, 130–135. 10.1016/s1471-4906(01)02168-8. [PubMed: 11864840]
45. Bolger AM, Lohse M, and Usadel B (2014). Trimmomatic: a flexible trimmer for Illumina sequence data. Bioinformatics 30, 2114–2120. 10.1093/bioinformatics/btu170. [PubMed: 24695404]
46. Kim D, Paggi JM, Park C, Bennett C, and Salzberg SL (2019). Graph-based genome alignment and genotyping with HISAT2 and HISAT-genotype. Nat. Biotechnol 37, 907–915. 10.1038/s41587-019-0201-4. [PubMed: 31375807]
47. Anders S, Pyl PT, and Huber W (2015). HTSeq--a Python framework to work with high-throughput sequencing data. Bioinformatics 31, 166–169. 10.1093/bioinformatics/btu638. [PubMed: 25260700]
48. Larkin A, Marygold SJ, Antonazzo G, Attrill H, Dos Santos G, Garapati PV, Goodman JL, Gramates LS, Millburn G, Strelets VB, et al. (2021). FlyBase: updates to the Drosophila melanogaster knowledge base. Nucleic Acids Res. 49, D899–d907. 10.1093/nar/gkaa1026. [PubMed: 33219682]
49. Mi H, Ebert D, Muruganujan A, Mills C, Albou LP, Mushayamaha T, and Thomas PD (2021). PANTHER version 16: a revised family classification, tree-based classification tool, enhancer regions and extensive API. Nucleic Acids Res. 49, D394–d403. 10.1093/nar/gkaa1106. [PubMed: 33290554]
50. Szklarczyk D, Gable AL, Lyon D, Junge A, Wyder S, Huerta-Cepas J, Simonovic M, Doncheva NT, Morris JH, Bork P, et al. (2019). STRING v11: protein-protein association networks

with increased coverage, supporting functional discovery in genome-wide experimental datasets. Nucleic Acids Res. 47, D607–d613. 10.1093/nar/gky1131. [PubMed: 30476243]

Highlights

- Many antimicrobial peptides and heat shock proteins are activated in poly(GR) flies
- Knockdown of Mtk partially rescues poly(GR)-induced toxicity in *Drosophila* neurons
- Hsp90 knockdown suppresses poly(GR) toxicity in flies and death of patient neurons
- Hsp90 and Mtk are regulated by TopoII, another suppressor of poly(GR) toxicity

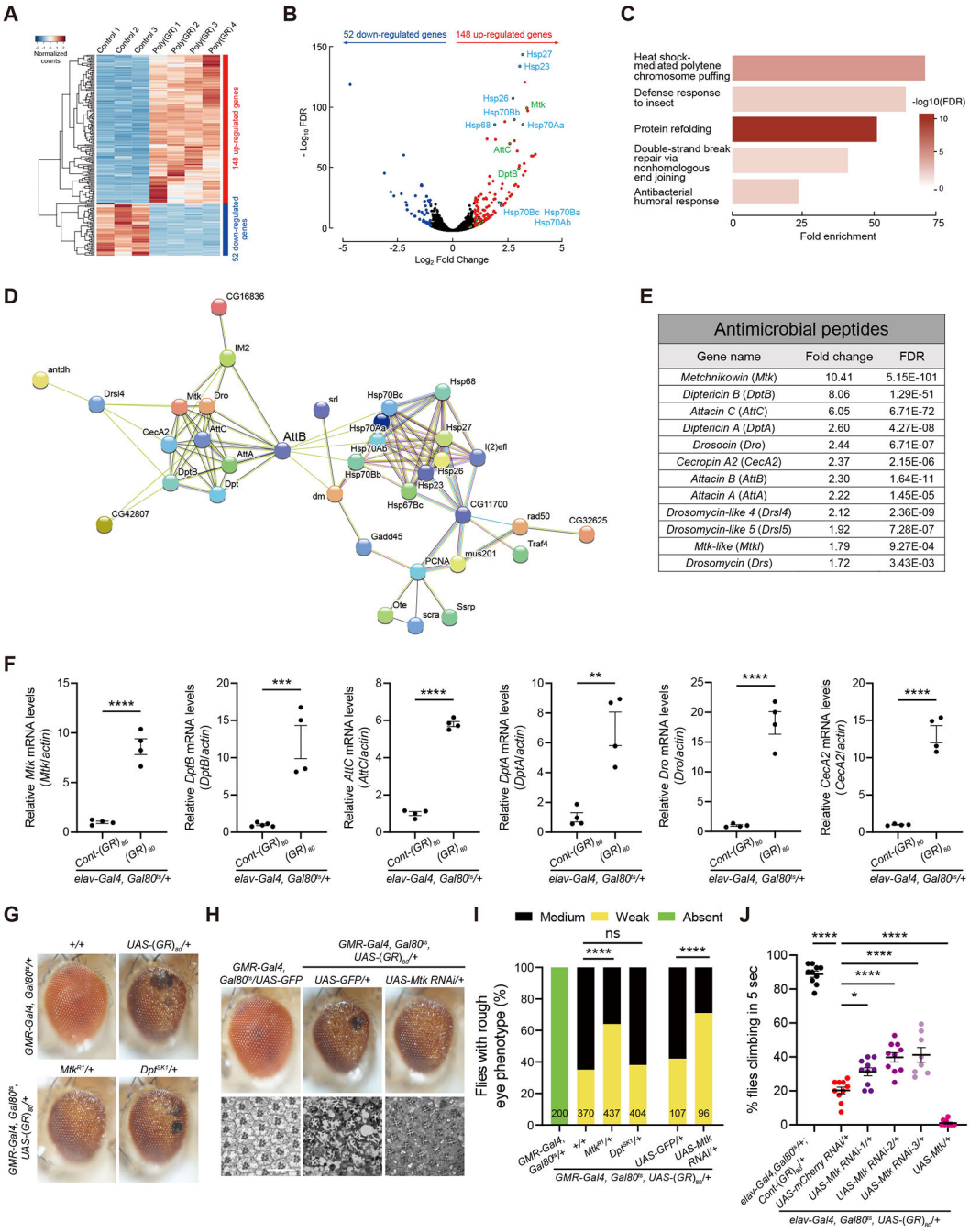

Figure 1. RNA-Seq analysis identifies overactivated AMP gene *Mtk* as a contributing factor to poly(GR) toxicity in *Drosophila*

(A) Hierarchical clustering heatmap showing the relative expression of differentially expressed genes in the heads of 3-week-old flies expressing *Cont-(GR)$_{80}$* or *(GR)$_{80}$* driven by *elav-Gal4. UAS-Cont-(GR)$_{80}$* expresses *(GR)$_{80}$* mRNA but the start codon AUG is changed into the stop codon UAA. Each sample is from an independent cross, n=3, 4 independent crosses.

(B) Volcano plot depicting the −log10 *p*-value vs log2 fold change of genes between controls and poly(GR). Genes with FDR <0.05 and log2 FC >1 are shown in red. Genes with FDR <0.05 and log2 FC <−1 are shown in blue. Genes of particular interest are labeled.
(C) Top enriched Gene Ontology (GO) terms of biological processes for upregulated differentially expressed genes in poly(GR)-expressing flies compared to control.
(D) Protein-protein interactions for upregulated genes identified through the STRING database (https://string-db.org/). Only proteins with connections are shown.
(E) Table showing upregulated antimicrobial peptide (*AMP*) genes in a poly(GR)-expressing fly model.
(F) Validation of RNA-seq data of *Mtk*, *DptB*, *AttC*, *DptA*, *Drosocin*, and *CecA2* genes expression by RT-qPCR in the head of 3-week-old male flies expressing poly(GR) under *elav-GAL4*. The *P* value was determined by two-tailed Student-*t* test. n=4, each from an independent genetic cross and mRNA measurement.
(G) Representative images of adult eye phenotypes of different genotypes showing partial inhibition of poly(GR) toxicity by decreasing Mtk activity but not DptB. Flies were crossed to a w^{1118} control strain.
(H) External and internal eye phenotypes of poly(GR) flies are partially blocked by Mtk depletion. Toluidine blue staining of eye cross-sections shows the structure of rhabdomeres. *UAS-GFP* was used for control for genetic crosses with other *UAS* elements. Scale bar 25 uM.
(I) Quantification of the genetic effects of *Mtk* and *DptA/B* on the rough eye phenotype caused by poly(GR). The number of flies of each genotype is shown in each column. The *P* value was determined by chi-square test.
(J) Control and pan-neuronal poly(GR)-expressing male flies with or without *Mtk* modulation were analyzed by negative geotaxis climbing assay. For each genotype, the climbing assay was performed in at least eight cohorts consisting of 14-21 flies per vial grown at 27 °C for 18 days (n=10, 10, 10, 8 and 10 vials respectively, Tukey–Kramer test). All data values are mean ± s.e.m. **** $p < 0.0001$, *** $P < 0.001$, ** $P < 0.01$, * $P < 0.05$, ns, not significant.
See also Figure S1.

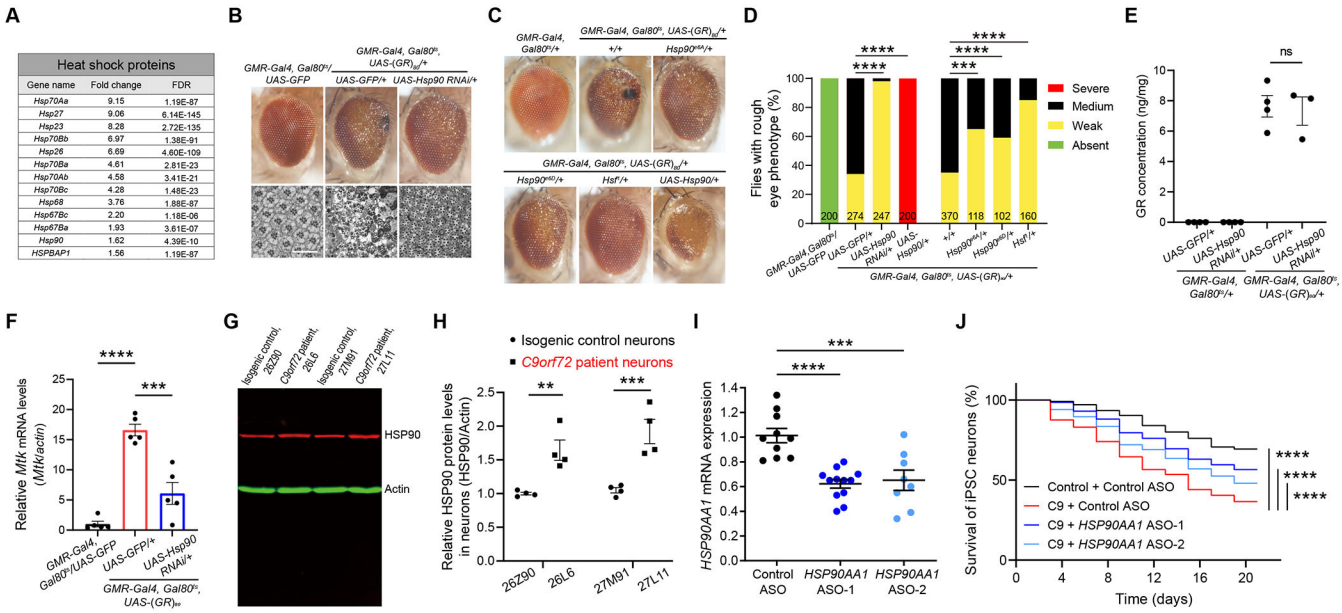

Figure 2. The AMP gene *Mtk* is activated by Hsp90, and inhibition of Hsp90 alleviates neurodegeneration in poly(GR)-expressing flies and *C9ORF72* iPSC-derived motor neurons

(A) Table showing upregulated HSPs in a pan-neuronal poly(GR)-expressing fly model.

(B) External and internal eye phenotypes of poly(GR) flies are dramatically rescued by Hsp90 knockdown. Sectioned adult eyes stained with toluidine blue. *UAS-GFP* was used for control for genetic crosses with other *UAS* elements. Scale bar 25 uM.

(C) Representative images of adult eye phenotypes in flies of different genotypes showing suppression of poly(GR) toxicity by genetic reduction or overexpression of Hsp90 activity. Flies were crossed to a w^{1118} control strain.

(D) Quantification of the suppressor effects of Hsp90 on the eye degeneration phenotype caused by poly(GR). The number of flies of each genotype is presented in each column. The *P* value was determined by chi-square test.

(E) *Hsp90* knockdown does not change poly(GR) protein levels in the fly head. One-way ANOVA with Tukey post-hoc test for multiple comparisons.

(F) Elevated *Mtk* expression level is dramatically attenuated by *Hsp90* knockdown in poly(GR)-expressing flies. One-way ANOVA with Tukey post-hoc test for multiple comparisons. *UAS-GFP* was used as control for genetic crosses with other *UAS* elements.

(G and H) Western blot analysis (G) and quantification (H) of HSP90 level in 3-month-old control and *C9ORF72* iPSC-derived motor neurons. $n = 4$, two-way ANOVA and Bonferroni post-hoc test.

(I) Quantification of the efficiency of *HSP90AA1* ASOs knockdown in iPSC-derived motor neurons. One-way ANOVA with Dunnett's post-hoc test for multiple comparisons.

(J) Decreased survival of *C9ORF72*-ALS patient iPSC-derived motor neurons upon withdrawal of neurotrophic factors is partially rescued by *HSP90AA1* ASO treatment. Three biologically independent iPSC lines were differentiated ($n = 100$ neurons per condition). All motor neuron survival experiments were analyzed by two-sided log-rank test, and statistical significance was calculated from the entire survival time course. All data values are mean ± s.e.m. **** $P < 0.0001$, *** $P < 0.001$, ** $P < 0.01$, * $P < 0.05$, ns, not significant.

See also Figure S2.

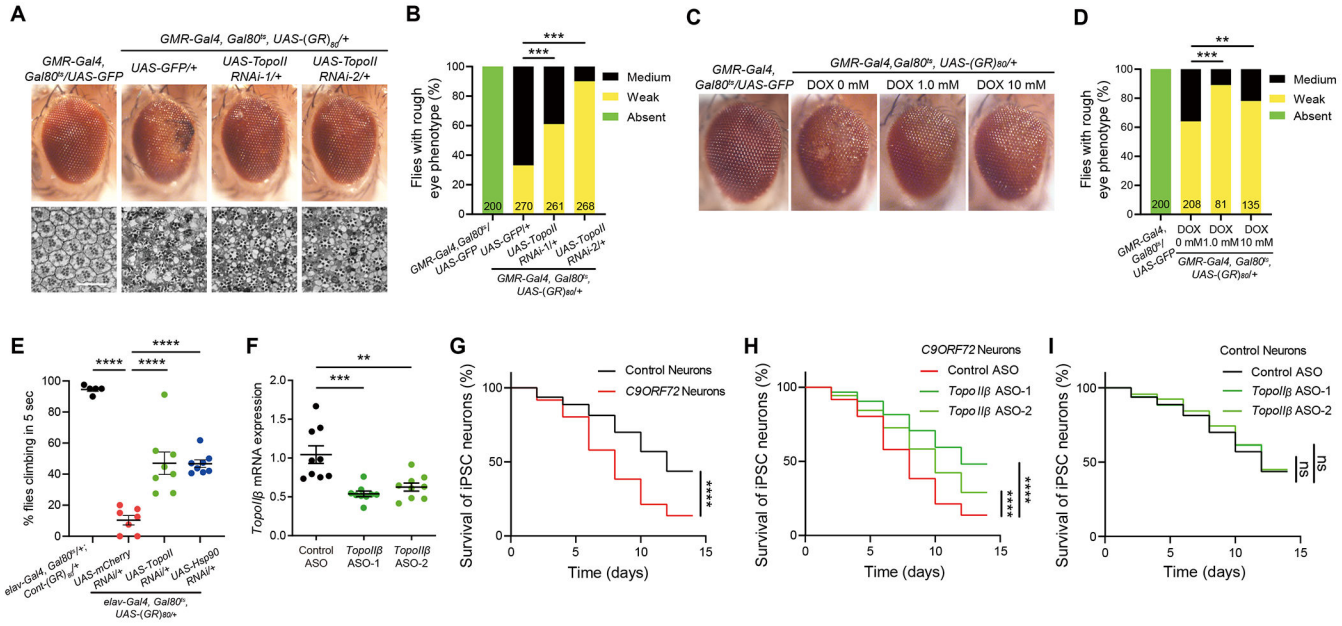

Figure 3. Partial loss of TopoII activity suppresses poly(GR) toxicity in flies and neurodegeneration in *C9ORF72* iPSC-derived motor neurons

(A) Genetic knockdown of *TopoII* strongly suppresses poly(GR) toxicity in *Drosophila* photoreceptor neuron. Representative images of adult external and internal eye phenotypes of flies with different genotype. *UAS-GFP* was used as control for genetic crosses with other *UAS* elements. Scale bar 25 uM.

(B) Quantification of the effects of *TopoII* knockdown on poly(GR)-induced external eye degeneration phenotype. The number of flies of each genotype is presented in each column. The *P* value was determined by chi-square test.

(C) Doxorubicin suppresses poly(GR)-induced toxicity in *Drosophila* eye. Representative images of eye phenotypes of control and $(GR)_{80}$ flies fed vehicle or doxorubicin.

(D) Quantification of the eye degeneration phenotype. The number of flies of each genotype is shown in each column. The *P* value was determined by chi-square test.

(E) Pan-neuronal downregulation of *TopoII* or *Hsp90* rescues the locomotor defect of $(GR)_{80}$ flies in negative geotaxis climbing assay. For each genotype, climbing assay was performed at least five cohorts consisting of 16-20 flies grown at 27 °C at 3 weeks (n=5, 7, 8, and 8, Tukey–Kramer test). *UAS-mCherry RNAi* was used as control for genetic crosses with other *UAS-RNAi* elements.

(F) Quantification of the efficiency of *TopoIIβ* ASOs knockdown in iPSC-derived motor neurons. One-way ANOVA with Dunnett's post-hoc test for multiple comparisons.

(G) Decreased survival of *C9ORF72* ALS patient motor neurons. Three control and three *C9ORF72* iPSC lines were differentiated (n = 100 neurons per line).

(H) Decreased survival of *C9ORF72* motor neurons was significantly increased by *TopoIIβ* ASOs treatment. Three *C9ORF72* iPSC lines were differentiated (n = 100 neurons per line).

(I) Survival of control iPSC-derived motor neurons treated with *TopoIIβ* ASOs or control ASO. Three iPSC lines were differentiated (n = 100 neurons per line). All motor neuron survival experiments were analyzed by two-sided log-rank test, and statistical significance

was calculated from the entire survival time course. All data values are mean ± s.e.m. **** $P < 0.0001$, *** $P < 0.001$, ** $P < 0.01$, * $P < 0.05$, ns, not significant.
See also Figure S3.

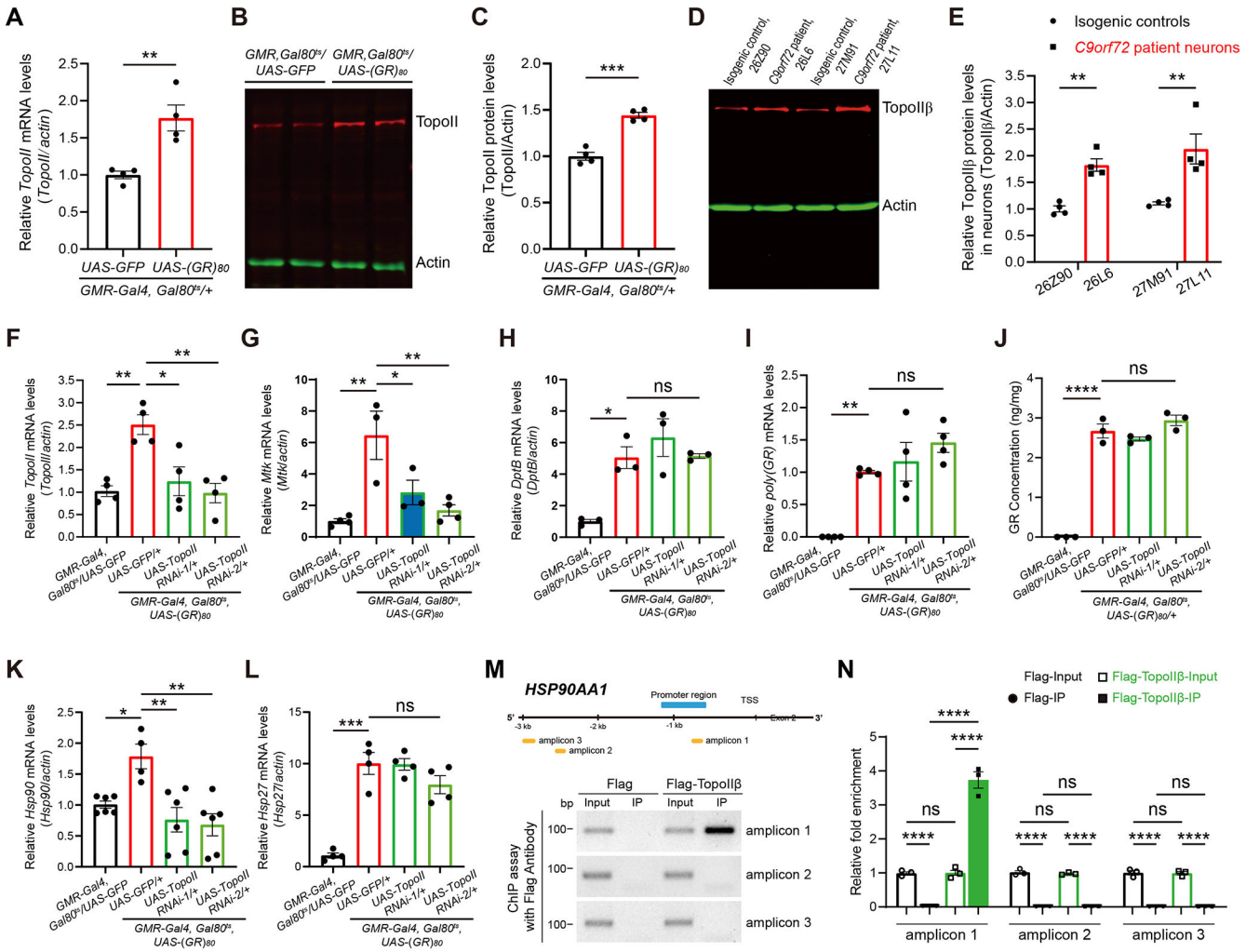

Figure 4. Upregulation of *Mtk* and *Hsp90* in poly(GR)-expressing flies is controlled by TopoII

(A) RT-qPCR analysis of *TopoII* expression in 10-day-old fly heads expressing poly(GR) under *GMR-Gal4* driver, $n = 4$, the *P* value was determined by two-tailed Student-*t* test.

(B and C) Western blot analysis (B) and quantification (C) of TopoII protein level in 10-day-old control and poly(GR)-expressing flies. *UAS-GFP* was used as control for genetic crosses with other *UAS* elements. $n = 4$, the *P* value was determined by two-tailed Student-*t* test.

(D and E) Western blot analysis (D) and quantification (E) of TopoIIβ protein level in 3-month-old control and *C9ORF72* iPS-derived motor neurons. $n = 4$, Two-way ANOVA and Bonferroni post-hoc test for multiple comparisons.

(F-H) RT-qPCR analysis of *TopoII* (F), *Mtk* (G), and *DptB* (H) mRNA levels in the heads of control and $(GR)_{80}$ flies with or without TopoII RNAi. *UAS-GFP* was used as control for genetic crosses with other *UAS* elements. $n \geq 3$, One-way ANOVA with Tukey post-hoc test for multiple comparisons.

(I and J) *TopoII* knockdown does not change poly(GR) mRNA level (I) and protein levels (J) in the fly head. One-way ANOVA with Tukey post-hoc test for multiple comparisons.

(K and L) RT-qPCR analysis of *Hsp90* (K) and *Hsp27* (L) mRNA levels in the heads of control and $(GR)_{80}$ flies with or without TopoII RNAi. *UAS-GFP* was used as control for genetic crosses with other *UAS* elements. $n \geq 4$, One-way ANOVA with Tukey post-hoc test for multiple comparisons.

(M) TopoIIβ ChIP assay of the human *HSP90AA1* gene. Schematic diagram of the human *HSP90AA1* promoter and amplicons used in the ChIP assay (upper). ChIP-qPCR showing TopoIIβ binding to the indicated sites in HEK293T Cells (bottom).

(N) Quantification of TopoIIβ binding to regions 1 to 3. One-way ANOVA with Tukey post-hoc test for multiple comparisons. All data values are mean ± s.e.m. **** $P < 0.0001$, *** $P < 0.001$, ** $P < 0.01$, * $P < 0.05$, ns, not significant.

See also Figure S4.

Key resources table

REAGENT or RESOURCE	SOURCE	IDENTIFIER
Antibodies		
Mouse anti-Hsp90	BD Biosciences	Cat#610419, RRID:AB_397799
Mouse anti-β actin	Santa Cruz Biotechnology	Cat#sc-47778, RRID:AB_626632
Mouse anti-β actin	DSHB	Cat# jla20, RRID:AB_528068
Rabbit anti-TOP2B	Novus	Cat#NBP1-89527, RRID:AB_11035093
Rabbit anti-TopoII	Buchenau et al., 1993	N/A
IRDye 680RD goat anti-rabbit	LI-COR Biosciences	Cat#926-68071
IRDye 800RD donkey anti-mouse	LI-COR Biosciences	Cat#926-32212
Chemicals, peptides, and recombinant proteins		
Doxorubicin hydrochloride	Sigma-Aldrich	Cat#D1515; CAS: 25316-40-9
Critical commercial assays		
miRNeasy Kit	Qiagen	Cat#74106
TaqMan Reverse Transcription Kit	Thermo Fisher Scientific	Cat#N8080234
SYBR Select Master Mix	Thermo Fisher Scientific	Cat#4472918
ChIP kit	Abcam	Cat#ab500
Experimental models: Cell lines		
Human: HEK293T cells	ATCC	Cat#CRL-11268
Human: Isogenic control line 26Z90	Lopez-Gonzalez et al., 2019	N/A
Human: Isogenic control line 27M91	Lopez-Gonzalez et al., 2019	N/A
Human: *C9ORF72* carrier 26L6	Almeida et al., 2013	N/A
Human: *C9ORF72* carrier 27L11	Almeida et al., 2013	N/A
Human: control line 1 (CTRL-1)	NINDS Biorepository at the Coriell Institute	Cat#ND03231
Human: control line 2 (CTRL-2)	NINDS Biorepository at the Coriell Institute	Cat#ND03719
Human: control line 3 (CTRL-3)	NINDS Biorepository at the Coriell Institute	Cat#ND05280
Human: *C9ORF72*-ALS line 1 (C9 ALS-1)	NINDS Biorepository at the Coriell Institute	Cat#ND06769
Human: *C9ORF72*-ALS line 2 (C9 ALS-2)	NINDS Biorepository at the Coriell Institute	Cat#ND10689
Human: *C9ORF72*-ALS line 3 (C9 ALS-3)	NINDS Biorepository at the Coriell Institute	Cat#ND12099
Experimental models: Organisms/strains		
D. melanogaster: GMR-Gal4: w[1118]; P{GMR-GAL4.w[-]}2/CyO	Bloomington Drosophila Stock Center	BDSC:9146; FlyBase: FBti0072862
D. melanogaster: elav-Gal4: P{w[+mC]=GAL4-elav.L}2/CyO	Bloomington Drosophila Stock Center	BDSC:8765; FlyBase: FBti0072909
D. melanogaster: Tub-Gal80^{ts}: w[*]; P{w[+mC]=tubP-GAL80[ts]}20; TM2/TM6B, Tb[1]	Bloomington Drosophila Stock Center	BDSC:7019; FlyBase: FBti0027796
D. melanogaster: UAS-GFP	Yang et al., 2015	N/A

REAGENT or RESOURCE	SOURCE	IDENTIFIER
D. melanogaster: UAS-mCherry-RNAi: y[1] sc[*] v[1] sev[21]; P{VALIUM20-mCherry}attP2	Bloomington Drosophila Stock Center	BDSC:35785; FlyBase: FBti0143385
D. melanogaster: w^{1118}	Bloomington Drosophila Stock Center	BDSC:3605; FlyBase: FBal0018186
D. melanogaster: UAS-Mtk-RNAi-1: w[1118]; P{GD3790}v8792/TM3	Vienna Drosophila Resource Center	VDRC:8792; FlyBase: FBst0471250
D. melanogaster: UAS-Mtk-RNAi-2: P{KK113189}VIE-260B	Vienna Drosophila Resource Center	VDRC:109740; FlyBase: FBst0481400
D. melanogaster: UAS-Mtk-RNAi-3: y[1] v[1]; P{TRiP.HM05032}attP2/TM3, Sb[1]	Bloomington Drosophila Stock Center	BDSC:28546; FlyBase: FBst0028546
D. melanogaster: UAS-Hsp23-RNAi-1: y[1] v[1]; P{TRiP.HMS06055}attP40	Bloomington Drosophila Stock Center	BDSC:82961; FlyBase: FBti0201590
D. melanogaster: UAS-Hsp23-RNAi-2: y[1] sc[*] v[1] sev[21]; P{TRiP.HMS02745}attP40	Bloomington Drosophila Stock Center	BDSC:44029; FlyBase: FBti0158629
D. melanogaster: UAS-Hsp26-RNAi-1: P{KK106347}VIE-260B	Vienna Drosophila Resource Center	VDRC: 100955; FlyBase: FBst0472828
D. melanogaster: UAS-Hsp26-RNAi-2: y[1] sc[*] v[1] sev[21]; P{TRiP.GL00329}attP2	Bloomington Drosophila Stock Center	BDSC:35408; FlyBase: FBti0144411
D. melanogaster: UAS-Hsp27-RNAi-1: y[1] sc[*] v[1] sev[21]; P{TRiP.HMS00807}attP2	Bloomington Drosophila Stock Center	BDSC:33007; FlyBase: FBti0140519
D. melanogaster: UAS-Hsp27-RNAi-2: y[1] sc[*] v[1] sev[21]; P{TRiP.HMS00867}attP2	Bloomington Drosophila Stock Center	BDSC:33922; FlyBase: FBti0140576
D. melanogaster: UAS-Hsp70-RNAi: y[1] sc[*] v[1] sev[21]; P{TRiP.GLV21036}attP2	Bloomington Drosophila Stock Center	BDSC:35671; FlyBase: FBti0144632
D. melanogaster: UAS-Hsp90-RNAi: y[1] sc[*] v[1] sev[21]; P{TRiP.HMS00899}attP2	Bloomington Drosophila Stock Center	BDSC:33947; FlyBase: FBti0140605
D. melanogaster: UAS-Hsp90: y[1] w[*]; PBac{y[+mDint2] w[+mC]=UAS-Hsp83.Z}VK00037	Bloomington Drosophila Stock Center	BDSC:58469; FlyBase: FBti0163127
D. melanogaster: $Hsp90^{e6A}$: w[*]; Hsp83[e6A]/TM6B, Tb[1]	Bloomington Drosophila Stock Center	BDSC:36576; FlyBase: FBal0029644
D. melanogaster: $Hsp90^{e6D}$: w[*]; Hsp83[e6D]/TM3, Sb[1]	Bloomington Drosophila Stock Center	BDSC:5696; FlyBase: FBal0029645
D. melanogaster: Hsf^{1}: net[1] cn[1] Hsf[1]/CyO	Bloomington Drosophila Stock Center	BDSC:5491; FlyBase: FBal0044857
D. melanogaster: UAS-TopoII-RNAi-1: y[1] v[1]; P{TRiP.JF01300}attP2	Bloomington Drosophila Stock Center	BDSC:31342; FlyBase: FBti0130747
D. melanogaster: UAS-TopoII-RNAi-2: y[1] sc[*] v[1] sev[21]; P{TRiP.GL00338}attP2	Bloomington Drosophila Stock Center	BDSC:35416; FlyBase: FBti0144419
D. melanogaster: Dpt^{SK1}	Hanson et al., 2019	N/A
D. melanogaster: Mtk^{R1}	Hanson et al., 2019	N/A
D. melanogaster: UAS-Mtk	Cao et al., 2013	N/A
D. melanogaster: GMR-Gal4, Tub-GAL80^{ts}, UAS-$(GR)_{80}$/CyO	Lopez-Gonzalez et al., 2019	N/A
D. melanogaster: elav-Gal4, Tub-Gal80^{ts}/CyO; UAS-Control-$(GR)_{80}$/TM6B, Tb	Yuva-Aydemir et al., 2019	N/A
D. melanogaster: elav-Gal4, Tub-Gal80^{ts}, UAS-$(GR)_{80}$/CyO	Yuva-Aydemir et al., 2019	N/A
Oligonucleotides		
See Table S2 for Oligonucleotides		
Recombinant DNA		

REAGENT or RESOURCE	SOURCE	IDENTIFIER
Plasmid: p3xFLAG-CMV™-7.1	Sigma-Aldrich	Cat#E7533
Plasmid: pCMV-3xFLAG-TopoIIβ	This paper	N/A
Hb9::RFP+ lentiviral vector	Addgene	Cat#37081
Software and algorithms		
FIJI	NIH, USA	https://imagej.net/Fiji
Prism 9	GraphPad	https://www.graphpad.com/scientific-software/prism/
Zen	Zeiss	N/A
ImageStudio	Li-Cor	https://www.licor.com/bio/image-studio-lite/
Other		
Biorender for model preparations	Biorender	https://biorender.com/